Journal of Advanced Joining Processes 7 (2023) 100142

Contents lists available at ScienceDirect

Journal of Advanced Joining Processes

journal homepage: www.sciencedirect.com/journal/journal-of-advanced-joining-processes

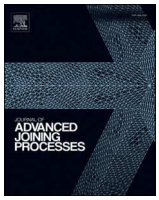

Correlation of surface and interfacial temperature during differential ultrasonic spot welding

Kaytie M. Barkley [a], Jaden S. Arner [a], Timothy A. Pike [a], Prasoon Diwakar [a], Cassandra M. Birrenkott [a,*]

[a] Department of Mechanical Engineering, South Dakota School of Mines and Technology, 501 East Saint Joseph Street, Rapid City, SD, 57701, United States of America

ARTICLE INFO

Keywords:
Ultrasonic spot welding
Differential ultrasonic spot welding
Thermoplastic polymers
Thermoplastic matrix composites
Infrared temperature measurement
Thermocouple

ABSTRACT

Ultrasonic spot welding (USW) has become an attractive joining method for thermoplastic polymers (TP) and thermoplastic matrix composites (TPMC). In the USW process, the material to be joined is subjected to mechanical vibrations of high frequency, causing intermolecular and surface friction which heat and melt the material at the joint interface. The interface resolidifies, resulting in a joint between two materials. In USW, it is necessary to focus the mechanical vibrations at the required weld location. A common method to accomplish this is to incorporate an energy director (ED) at the interface between materials to melt preferentially. However, incorporating EDs complicates the manufacturing process, particularly for large constant thickness polymer sheets. In this work, differential ultrasonic spot welding (DUS) is used which employs a flat horn and anvil of different diameters to initiate frictional heating between laminates at the desired joint location. This work investigates the effectiveness of DUS compared to a more traditional USW setup. Additionally, by measuring temperature at both the surface and the interface during DUS using infrared imaging and a thermocouple (TC), respectively, the driving factors behind the thermal profile of the welding process are examined. The goal of coupling the thermal profile to physical attributes of the DUS process is to eventually determine if variability present in the thermal profile may be tied to well-known joint area and strength variabilities.

Introduction

Polymer and composite materials have long had a strong connection to high-performance, lightweight products. The use of these materials has increased drastically in industries where materials must be strong and stiff, but also lightweight such as the sports, automotive, and aerospace industries.

For industry use, polymers are often used to create composite materials with customized strength and stiffness properties for given applications (Matthews and Rawlings, 1999). Polymeric matrices of composite materials consist of a material from one of two classes of polymers: thermosets (TS) or thermoplastics (TP). While TS's are often employed for their high strength and temperature resistance, this work focuses on TP matrix composites for their recently advanced attributes (Red, 2014). First, the manufacturing processes of TP's tend to be much simpler than that of TS's. TP's are melted at high processing temperatures, formed into the desired structure, and solidify as cooled (Balakrishnan et al., 2016). TS's have lower processing temperatures but require a long curing time during which irreversible chemical bonds are formed. Because of these bonds, TS's cannot melt and resolidify, but instead, degrade under high temperatures (Baur et al., 2016). Recyclability concerns surround the use of TS's as effective recycling methods are limited, while TP matrix composites can be melted and the reinforcement material and matrix separated and recycled individually (Yang et al., 2012). Recent advances in polymer chemistry have shown promise in circumventing the temperature limitations of TP's (Ageorges et al., 2001). Novel TP's, such as polyetherimide (PEI), polyether-ether-ketone (PEEK) and polyether-ketone-ether-ketone-ketone (PEKEKK) exhibit increased strength, high temperature resistance, and recyclability (Ageorges et al., 2001), making them ideal candidates for applications where TS's are traditionally employed.

TS's and TP's and their composites are often used in applications that require joining to create the end product, typically mechanical fastening or adhesive bonding. The holes created in mechanical fastening techniques introduce stress concentrations, lowering the overall strength of the component and complicating the manufacturing process (Costa

* Corresponding author.
E-mail address: cassandra.birrenkott@sdsmt.edu (C.M. Birrenkott).

https://doi.org/10.1016/j.jajp.2023.100142

Available online 11 April 2023

et al., 2012). Another downfall of joining composites with mechanical fasteners is the added weight of the fasteners, which are often made of metal. The increased weight of the component can decrease its efficiency, especially when considering use in the automotive or aerospace industries (Rana and Fangueiro, 2016). In place of mechanical bonding, adhesive bonding may also be used to join composite materials. Although stress concentrations from holes are avoided when using adhesives, extensive surface preparation is required, which complicates the manufacturing process (Costa et al., 2012).

Although current bonding mechanisms for composites have significant downfalls, the ability of TP material to melt and resolidify allows for the option of fusion bonding thermoplastic matrix composites (TPMCs). Fusion bonding is achieved by the melting of a polymer to join it with another as the material resolidifies (Ageorges et al., 2001) and is inherently limited to TP materials as TS's do not melt once initially formed. Fusion bonding is either achieved with bulk heating, which utilizes autoclaves and compression molding, or with frictional heating processes such as ultrasonic spot welding (USW), spin welding or vibrational welding (Newkirk et al., 2018). This work focuses on the USW process to create bonds between TP parts.

During the USW process, the welded material is subjected to mechanical vibrations of high frequency. These vibrations cause a transfer of energy to the material, which dissipates in the form of intermolecular and surface friction between the laminates. The interfacial surface friction heats and melts the material at the joint interface. Once the frictional heating dissipates, viscoelastic heating takes over for the reminder of the welding process. When welding has finished, the ultrasonic vibrations are discontinued, and the material is subjected to pressure under which re-solidification of the molten material occurs (Tutunjian et al., 2020).

The use of the USW joining technique can decrease or eliminate the need for mechanical fasteners and adhesive bonding – along with their respective disadvantages. Ideally, USW can create joints that have properties matching those of the parent material, offering the promise of a more efficient joining method as it avoids complex manufacturing processes of other joining processes, and can be highly automated (Tutunjian et al., 2020). For this work, a Dukane ultrasonic welder was utilized with available input parameters of weld time, applied pressure to the workpiece (0 – 0.69 MPa), amplitude of the weld horn (0 – 60 μm), and energy (calculated during welding).

Although USW is a promising advancement in joining composites and polymers, the strength and quality of the joints created are highly varied and difficult to characterize. Altering the parameters of the weld design greatly affects the welded bond area, and bonds created with the same set of parameters often vary widely in size and strength. One downfall of USW has been seen in the need for energy directors (ED) that are often incorporated between welded materials as seen in Fig. 1a to initiate preferential welding at the desired joint location (Ageorges et al., 2001; Yousefpour et al., 2004; Villegas and Bersee, 2010). However, incorporating EDs into the joint setup complicates the welding process as they are difficult to incorporate on sheets of material (Ageorges et al., 2001; Yousefpour et al., 2004; Villegas and Bersee, 2010). To circumvent this issue, USW can be done with a pointed weld tip as seen in Fig. 1b that penetrates the top sheet of material being welded. Friction occurs between the weld tip and the material, generating heat. However, the completed joint is left with a void at its center – introducing a stress concentration and decreasing the overall area of the joint (Barkley, 2021).

To avoid the negative issues created with each of the USW methods mentioned, this work explores a joint design called differential ultrasonic spot welding (DUS) that utilizes a flat, knurled welding tip, called a horn (diameter 14.4 mm) and anvil (diameter 10.2 mm) of differing diameters to initiate welding at the desired joint location (Tutunjian et al., 2018). The DUS setup can be seen in Fig. 2. This design results in joints created without the need to incorporate EDs, while also avoiding voids that would be introduced with a pointed weld tip.

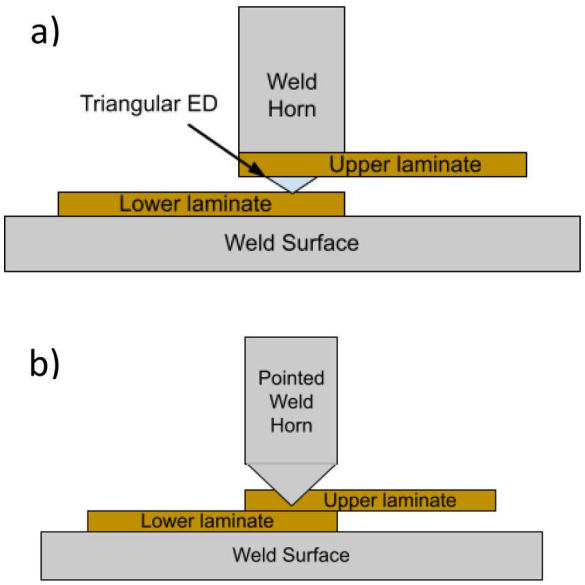

Fig. 1. Schematic of USW with the use of a) an energy director and b) a pointed weld tip (Villegas and Bersee, 2010).

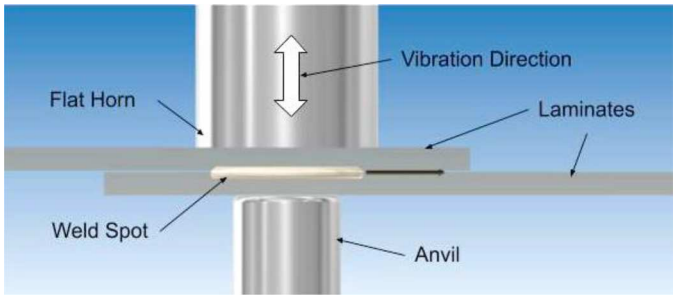

Fig. 2. Schematic of DUS utilizing a flat horn and anvil (Tutunjian et al., 2018).

In this work, TP joints were created via DUS and compared to joints created with a pointed weld tip to determine if DUS resulted in joints with increased and more consistent area and strength properties. Additionally, the surface and interface temperature development were measured and correlated to various steps that occur during DUS, with the goal of understanding if inconsistencies in the thermal profile that occurs during welding may be tied to the variation in joint area and strength commonly known as an issue for USW processes.

Thermoplastic selection and joint design

Due to their relevance in industry – particularly aerospace, this work investigates DUS of TP's. Specialized engineering TP's used in advanced applications require high temperature resistance, high impact strength, chemical resistance or some combination of specialized properties for a specific application (Fried, 2014). Some notable engineering thermoplastics already mentioned are PEI, PEEK, and PEKEKK (Fried, 2014). Of these three TP's, PEEK and PEKEKK are semi-crystalline, while PEI is amorphous. The crystallinity of a polymer is of interest because it effects how the polymer responds to heat. Semi-crystalline polymers have regularly structured polymer chains, which require thermal energy large enough to allow the chains to break free of the structure, leading to flow of the melting polymer. Amorphous TP's have no specific chain structure, which allows the chains to move with less thermal energy over a wider range of temperatures (Fried, 2014).

Because of a more gradual melting behavior, PEI TP (Curbell Plastics, Ultem®1000, tensile strength 121 MPa). was chosen for this work. The

amorphous behavior of PEI allowed a joint to be formed under a wider range of temperatures, due to the gradual melting that occurs rather than the abrupt phase change that is present in semi-crystalline polymers when the melting temperature (T_m) is reached.

When done with a flat horn, common USW methods utilize an ED as seen in Fig. 1a to initiate preferential heat generation. The material chosen for the ED often has a lower T_m than the material being welded, allowing it to melt and flow first, and resulting in a joint at the desired location. Although EDs aid in preferential flow, adding them to the joint setup is often tedious and complicates the manufacturing process (Ageorges et al., 2001; Yousefpour et al., 2004; Villegas and Bersee, 2010). To avoid incorporating an ED into the interface between welded laminates, a pointed weld tip can be incorporated, as seen in Fig. 1b. Utilizing a pointed weld tip allows for a joint to be formed without an energy director, but results in a void in the center of the created bond, as seen in Fig. 3.

To circumvent issues associated with USW with an ED and to prevent creating a void in the final bond joint, DUS welding was utilized in this work as seen in Fig. 2. Noteworthy of this setup is the small anvil diameter when compared with the diameter of the horn. This difference in diameters promotes bending in stages during applied ultrasonic vibration where the lap joint is compressed between the horn and anvil. This bending causes interfacial slippage to occur between the laminate interface surfaces, which generates frictional heating and successive melting initiating around the perimeter of the anvil (Tutunjian et al., 2020).

Analysis of weld characteristics

To determine the bond area and strength of the updated joint design, six weld coupons were created with welding parameters of 400 J of input energy, 0.27 MPa static pressure, and 24 μm amplitude of vibration. Earlier work created PEI TP and PEI TPMC joints welded with a pointed horn (Barkley, 2021). The areas of the welds were traced and measured using the software ImageJ. To measure the strength of the bonds, the PEI lap joints were pulled in tension using a dual actuated load frame to impart shear force across the bonded area. The lap joint coupons were pulled at a rate of 5 mm/min based on ASTM D638 (Barkley, 2021; International, 2014). A side view schematic of the test coupons can be seen in Fig. 4.

Upon testing the welded PEI lap joints using the tension test depicted in Fig. 4, it was observed that the bond area of the weld rarely failed in shear, as would be typical of pulling lap joints in tension. Rather, the break occurred at the weld root, pictured in Fig. 5. This type of failure is indicative of Pullout Failure II (PFII) which is associated with strong lap joints that fail due to bending while under tension, rather than failing in tension or shear (Zhao et al., 2018; Junior et al., 2014). Because the lap joints did not fail through the area of the weld, the maximum failure load recorded during lap shear testing was used to characterize joint strength, rather than the computed stress (Newkirk et al., 2018; Villegas and Rans, 2021).

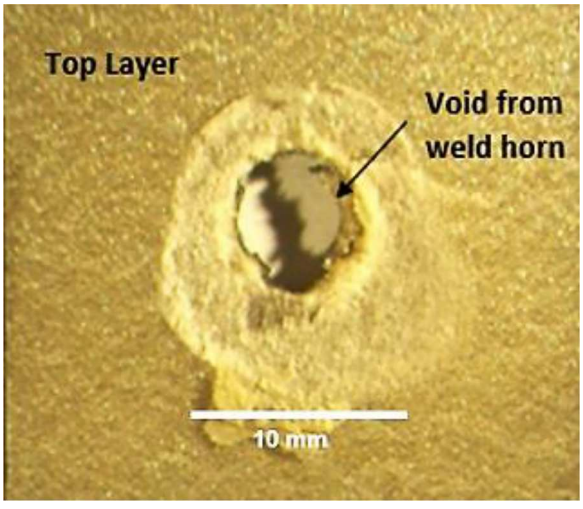

Fig. 3. Top view of PEI composite joint created with USW utilizing a pointed weld tip.

The measured average area of the DUS welds were compared to welds created with the pointed weld tip utilizing PEI TP and PEI TPMC with 30% glass fiber (Barkley, 2021). A comparison of the area and strength of the previously welded PEI composite lap joint and the area of PEI TP samples (Barkley, 2021) with the PEI TP lap joint created in this work can be seen in Table 1.

As seen in Table 1, although the joints created with the new USW setup were made purely of PEI TP material, they resulted in stronger maximum loads than the composite PEI joints made with the USW setup utilizing a pointed weld tip. In addition, the areas of welds created with DUS were larger and were more consistent than the measured areas of both the PEI composite and TP created with the pointed tip setup. The PEI TP welds created with DUS had a larger area, were stronger, and had a lower standard deviation in area and strength, which resulted in higher weld consistency. It is believed that the higher consistency in weld area and strength may also be linked to a more consistent temperature profile for DUS welding than that which would occur in USW with a pointed weld tip.

Investigation of the thermal profile during DUS

Due to the viscoelastic nature of TPMCs and TPs, it was hypothesized that the temperature profile that occurs during USW affects the flow of molten material at the weld location (Fried, 2014), affecting the final bond area and therefore the final strength of the weld. The unknown nature of the temperature profile during USW may be responsible for highly varied bond areas that are closely tied to weld strength, decreasing the abundant use of USW in industry. In addition, temperature spikes that occur during the welding process may be responsible for degradation of the polymeric material, resulting in a weaker joint.

To measure the temperature profile during DUS, a FLIR a655sc infrared thermal camera was used to record surface temperatures of PEI laminates during welding. Since the thermal camera is limited to recording visible portions of the top laminate's surface during welding, an OMEGA CHAL-003 thermocouple (Zhang et al., 2010) was placed at the interface of the weld to record interfacial temperatures. By utilizing the two methods to simultaneously measure temperatures, a through thickness comparison of recorded surface and interface temperatures could be achieved. A schematic of the experimental setup used to record surface and interface temperatures can be seen in Fig. 6.

To record accurate surface temperature readings, the FLIR a655sc camera was calibrated through a series of multiple tests. The emissivity of PEI was found to be 0.95 by measuring the actual temperature of the PEI using a thermocouple and measuring the object temperature with the FLIR camera and adjusting the emissivity setting until the correct value was reached. However, the emissivity of a material is susceptible to change when it experiences an increase in temperature (Marla et al., 2007; Fujikura, 1999). This effect could be seen for the case of PEI when the temperature increased enough that the polymer surface became glossy. To determine how largely this change in surface finish affects the temperature readings of PEI, experiments were run using a proportional integral derivative (PID) controller and a heating element to heat the polymer to a set temperature. The PEI temperature measurements started at room temperature, and the temperature was increased in increments of 5 °C, until a maximum reliable temperature of 225 °C was reached. Each time the temperature was increased, the polymer was allowed to stabilize for two minutes before the temperatures were measured with the TC and thermal camera. During the heating process, the emissivity of the camera was set to 0.95 and the accuracy of the

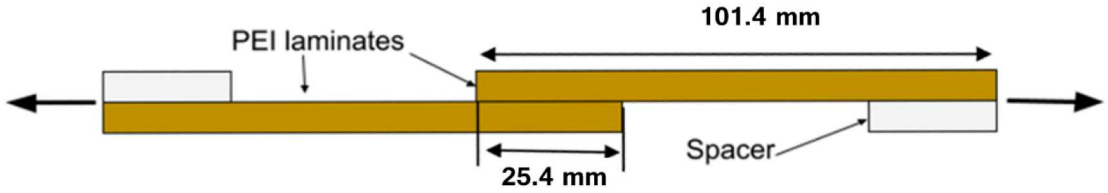

Fig. 4. Side view schematic of the shear test performed on welded lap joints.

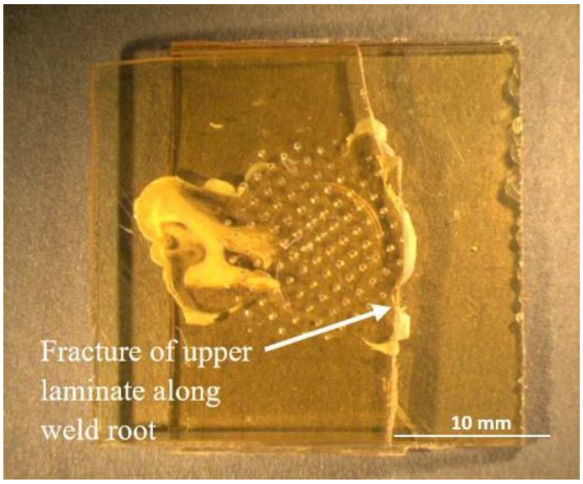

Fig. 5. Broken PEI sample showing failure at the weld root.

Table 1
Experimental data from DUS horn and anvil joint design compared to results utilizing a pointed weld tip (Barkley, 2021).

Weld material	Weld setup	Weld area (mm^2) ± 1 std dev	Load at break (N) ± 1 std dev
PEI Thermoplastic	DUS horn and anvil	168 ± 24	2127 ± 225
PEI Thermoplastic	Pointed tip	115 ± 42	not available
PEI GF Composite	Pointed tip	111 ± 36	1445 ± 410

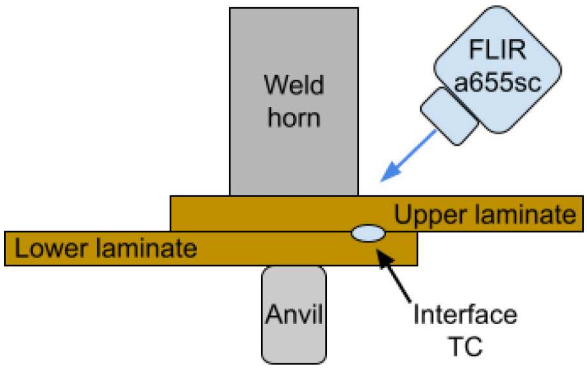

Fig. 6. A schematic of the simultaneous temperature recording at the surface and interface during DUS.

camera measurements were compared to the PID controller setting. Because USW takes place over a short period (≈1–2 s), it is not possible to adjust the emissivity of the thermal camera during the welding process. Therefore, a calibration curve was needed to determine at what temperatures the set emissivity became inaccurate, allowing temperatures recorded by the camera to be corrected post welding.

In addition, the OMEGA Chal-003 K-type TC was placed between the heating element and the PEI laminate, and the TC temperature was recorded using an Arduino UNO. This was done to compare the accuracy of the TC to the temperature setting of the PID controller. An image of the calibration test setup can be seen in Fig. 7. A plot of the thermal camera and TC readings compared with the set PID temperature can be seen in Fig. 8. It was evident that the measurements from the TC followed a very similar trend to ideal calibration, whereas the measurements taken with the thermal camera steadily deviated from the PID controller setting early in the test.

A linear trendline was fit to the FLIR cursor data and Eq. (1) was created to adjust FLIR temperatures above room temperature to match the ideal calibration line, $X = Y$. In this equation, T_c is the corrected temperature, and T_m is the temperature originally measured by the FLIR camera.

$$T_c = T_m * 1.14 - 1.37^{\circ}C \quad (1)$$

The interface directly above the perimeter of the anvil is defined as the weld apex, depicted in Fig. 9, and is the location where heat generation develops the quickest (Tutunjian et al., 2020). However, in order to compare the interface TC to the FLIR camera readings, the interface TC was moved further away from the weld apex, where the surface of the top laminate was not covered by the horn and could be visualized by the FLIR camera as seen in Fig. 6. At this location, the TC temperature readings were directly beneath the location of the thermal camera measurements, allowing for a through-thickness comparison of the surface and interface temperatures during welding. The TC chosen had a diameter of 0.075 mm which was assumed to be small enough to record interface temperatures without affecting the temperature profile of the weld (Zhang et al., 2010).

To record the surface and interface temperature profiles simultaneously during DUS, a National Instruments (NI) Data Acquisition (DAQ) system was used. Timestamps from the computer's internal clock were used to synchronize the temperature profiles with each other. The maximum sampling rate of the interface TC achieved was 7 Hz whereas the FLIR thermal camera was able to record surface temperatures at a sampling rate of 200 Hz.

To tie the physical welding steps to specific portions of the temporal profile, three welds were created with parameters of 400 J, 0.27 MPa, and 40% (24 μm) amplitude. The welding process for each of these tests was recorded with a video camera, and the recording was tied to the development of the temporal profile. The video was divided into several steps that occur during welding: 1) downward horn stroke, 2) pressure applied to the workpiece, 3) ultrasonic vibration applied, 4) holding pressure applied, and 5) horn lifted from the workpiece. The duration of each step was determined by analyzing visual and audio cues in a video editing software and synchronized with the FLIR and TC data to determine approximately which aspects of the temperature profile are caused by which physical welding step. From the visual and audio cues, it was observed that ultrasonic vibrations likely cause the sudden initial increase in the interface temperature profile. Therefore, the rapid increase at the beginning of the interface temperature profile was assumed to be correlated to the initiation of ultrasonic vibration (step 3 of the welding process). The interfacial temperature profiles of multiple tests were able to be synchronized based on this rapid increase. Fig. 10 depicts data from three DUS tests synchronized with this method.

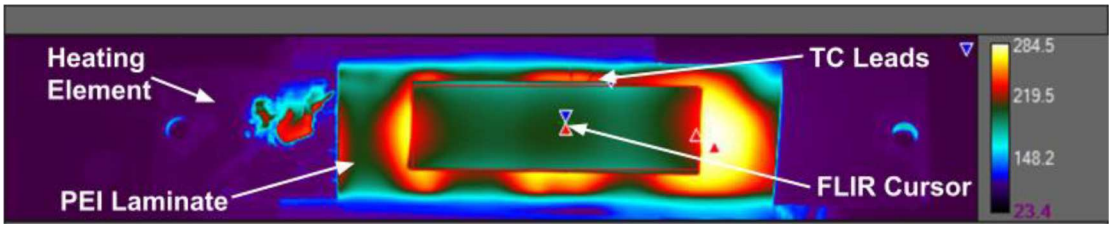

Fig. 7. Setup of the calibration test for the interface TC and FLIR thermal camera.

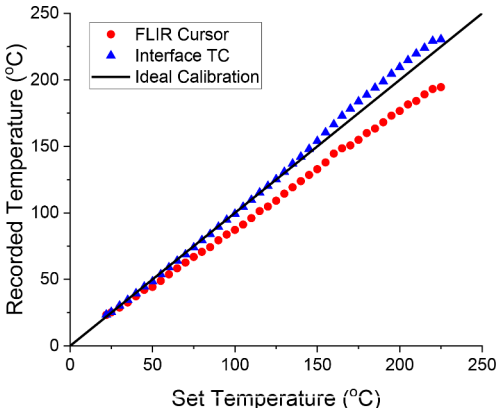

Fig. 8. Thermal camera and interface TC readings compared to PID setting used to create a correction factor for infrared measurements.

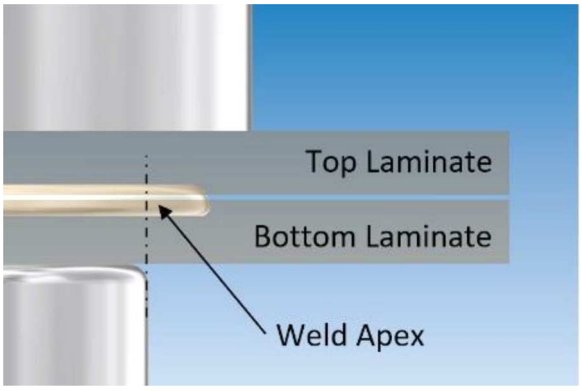

Fig. 9. Location of the weld apex.

It was also observed that the duration of the ultrasonic vibration from the recorded video closely corresponded with the output time given by the welder. For tests 1–3 the duration of ultrasonic vibration was recorded as 1.684 s, 1.709 s, and 1.554 s, respectively. When analyzing the data, the vibration time given by the welder was used to correlate the temperature profile to ultrasonic vibrations. Lastly, the duration of the holding pressure was a setting input to the welder as 1.5 s. Because the pre-weld holding pressure is not a known value, the video recording mainly served to determine at what point the ultrasonic vibrations began, as well as verify the output of the duration of the vibrations from the welder's power supply and the setting of the post-welding holding pressure.

Fully characterized temporal profile created during DUS

The glass transition temperature (T_g) and degradation temperature (T_d) of PEI were determined to be 220 °C and 450 °C, respectively based on Differential Scanning Calorimetry (DSC), Dynamic Mechanical Analysis (DMA), and Thermogravimetric Analysis (TGA) experiments completed at a 5 °C ramp rate. By utilizing the characteristic temperatures T_g and T_d tied to PEI material properties and the characteristic times determined from observations of the welding process, a fully characterized temperature profile of the DUS process was determined.

To correlate the physical welding steps to respective portions of the temperature profile, Test 2 from Fig. 10 was chosen as a representative sample. The predicted durations of each step of the welding process were overlayed on the time-temperature data using different colors to make a clearer connection between the temperature profile and the welding process. Fig. 11 shows the surface and interface temperature profiles measured from a PEI weld with discrete welding steps.

Although only depicted in Fig. 11 for a representative sample, it was observed that for each test, the white region corresponding to the horn lowering to the laminate surface was observed to have a no change in temperature. The green region correlated to pre-welding applied pressure continued to read a steady interface temperature as pressure was applied, whereas the surface increased slightly in temperature. This increase in surface temperature from the FLIR camera was likely due to inaccurate temperature readings caused by the reflective surface of the weld horn. The yellow region correlated to the duration of the ultrasonic vibration was observed to measure interface temperatures that increased rapidly with the initiation of the ultrasonic vibration. This rapid increase, denoted in literature as the rise time, was followed by a brief plateau before temperatures again rose to the maximum temperature that occurred during welding (Tutunjian et al., 2020). In addition, the interface began cooling as the ultrasonics turned off and post-weld pressure was applied, and as the horn lifted from the surface. Another observation made was that the surface temperatures rose slowly during ultrasonic vibration but continued to increase post welding so that the measurement from the TC and FLIR camera began to converge as temperature through the thickness of the sample became more consistent. From these observations, the experimentally determined temperature profile and the related physical welding steps were correlated.

Due to the low sampling rate of the interface TC, the temperature profile near the glass transition temperature at the interface could not be measured. However, the measured temperature profiles could be compared to T_d = 450 °C to determine if degradation occurred during welding at the TC location. The average maximum temperature was recorded from the first three tests and was determined to be 421.8 °C. However, the large spread present in the maximum temperatures of these first three tests confirms the high variation present in USW of TP's. To further explore the variation in the maximum temperature measured by the interface TC, data from five other tests that measured interfacial temperatures was analyzed. Table 2 shows this maximum temperature readings from all eight recorded interfacial temperature profiles along with the standard deviation. From Table 2, it is seen that only Test 1 surpassed the degradation temperature at the location of the TC, while all others remained below T_d.

From Table 2, the average temperature from all eight tests was determined to be 383.0 °C, with a standard deviation of 64.3 °C. Although the average maximum temperature for the given weld setup is well below degradation, the high standard deviation verifies the high variation in the maximum temperature reached during USW. It should be noted that the degradation temperature discussed here was measured

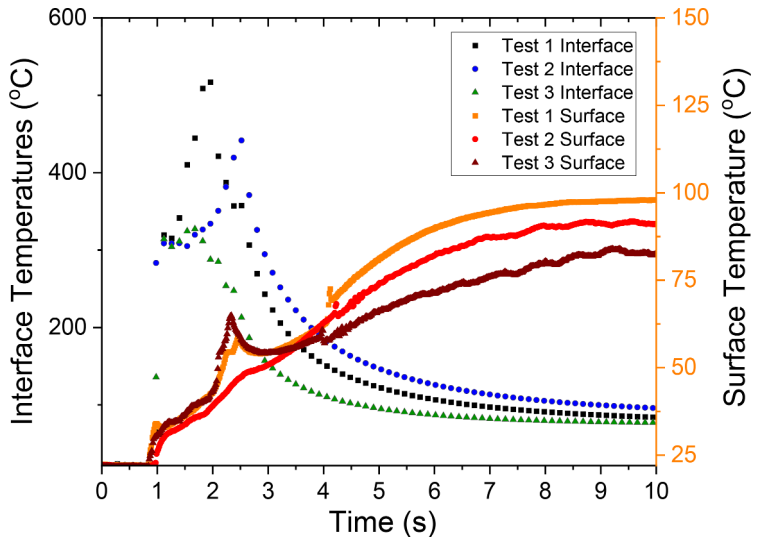

Fig. 10. Temperature profiles of USW for the duration of 3 DUS processes. Interface and surface temperature measured by the TC and FLIR thermal camera, respectively.

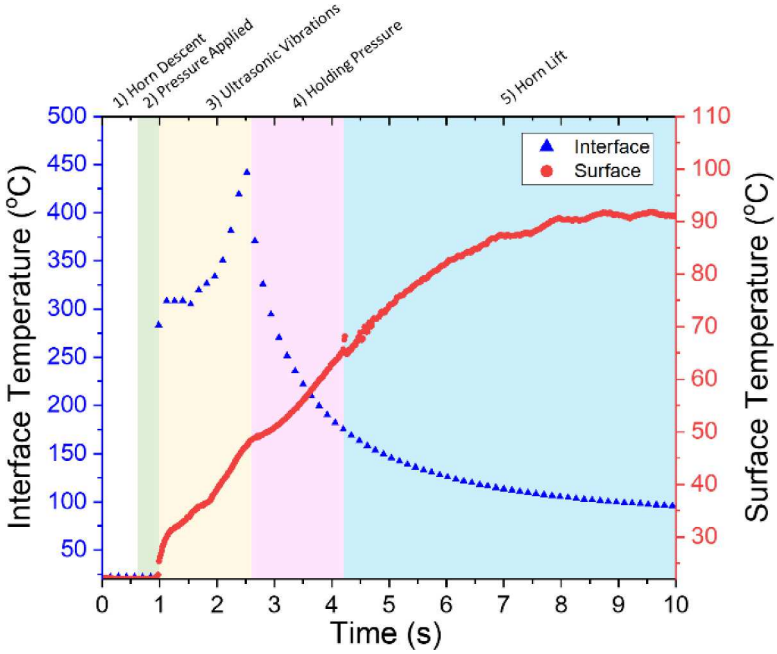

Fig. 11. Interface and surface profiles correlated to physical welding steps.

Table 2
Maximum interface temperatures recorded from 8 USW tests.

Test number	Maximum measured temperature (°C)
1	517.1
2	441.7
3	327.4
4	398.6
5	358.7
6	373.6
7	340.4
8	306.7
Average	**383.0 ± 64.3**

at a near steady-state through DSC, DMA, and TGA experiments. However, the very rapid rise of interface temperatures are likely to affect both the T_g and T_d, and further work is needed to verify these temperatures at heating rates seen during the USW process.

Conclusion

Utilizing the DUS method of USW was shown to successfully create welds without the need to incorporate tedious EDs that increase manufacturing time and cost. Additionally, the DUS method resulted in welds without a void present in the bond area and improved on this issue in USW with a pointed weld tip. Welds created with DUS were shown to create joints with larger average areas and maximum strength than those created with a pointed weld tip. DUS welds were also shown to be more consistent, and to result in PFII during tension tests – a fracture mechanism associated with strong lap joints.

The surface and interface temperature profiles that occur during DUS were recorded utilizing a thermal camera and interface TC. By synchronizing the temperature profiles and pairing them with various

stages of the welding process, a characterized temperature profile was developed that allowed for a better understanding temperature development during welding. It was observed that when ultrasonic vibration initiates, the interface between laminates heats very rapidly. This is likely due to interfacial friction that is generated from bending during compression stages of the welding process. Additionally, the maximum temperature occurring at the TC location was tied to the duration of the ultrasonic vibration. The duration of vibration was observed to vary from test to test and may be responsible for some of the variation measured between multiple thermal profiles. Lastly, it was observed that once ultrasonic vibrations are finished, the interface begins to cool very rapidly, whereas surface temperatures continue to increase as heat propagates through the thickness of the laminate, and the two temperature profiles begin to converge after DUS is completed.

This work utilized PEI TP laminates to validate the use of DUS to create higher quality welds while additionally providing a better understanding of the heating mechanisms present during the DUS so that future work may better understand how to avoid degradation of the TP material.

Declaration of Competing Interest

The authors have no known competing interests of financial or personal relationships that influenced the work reported.

Data availability

Data will be made available on request.

Acknowledgements

This work was supported by a NASA Space Technology Graduate Research Opportunity.

The authors would also like to thank the South Dakota Space Grant Consortium for support. Thanks also to the Joining and Mechanics of Polymers Laboratory at the South Dakota School of Mines where much of this work was performed. The researcher extends special thanks to the to South Dakota Mines faculty members, Dr. Peter McKeon, Dr. Nikolaus Bruno, Mr. Lowell Kolb, and Mr. Jason Ward for their assistance in performed experiments.

References

Ageorges, C., Ye, L., Hou, M., 2001. Advances in fusion bonding techniques for joining thermoplastic matrix composites: a review. Compos., Part A 32 (6), 839–857.

Balakrishnan, P., et al., Natural fibre and polymer matrix composites and their applications in aerospace engineering, in Advanced composite Materials For Aerospace Engineering. 2016, Elsevier. p. 365–383.

Barkley, C., 2021. Correlation of Experimental and Computational Models to Predict the Response of Thermoplastic Matrix Composite Lap Joints. Mechanical Engineering, South Dakota Mines.

Baur, E., K. Ruhrberg, and W. Woishnis, Chemical Resistance of Commodity Thermoplastics. 2016: William Andrew.

Costa, A.P.d., et al., 2012. A review of welding technologies for thermoplastic composites in aerospace applications. J. Aerosp. Technol. Manag. 4 (3), 255–265.

Fried, J.R., Polymer Science and Technology. 2014: Pearson Education.

Fujikura, Y. Emissivity of polymers. Yamagata Daigaku Kiyo, Kogaku 1999, 25 (2), 55–68.

International, A., Standard Test Method for Tensile Properties of Plastics. 2014: ASTM international.

Junior, W.S., Emmler, T., Abetz, C., Handge, U.A., Dos Santos, J.F., Amancio-Filho, S.T., Abetz, V, 2014. Friction spot welding of PMMA with PMMA/silica and PMMA/silica-g-PMMA nanocomposites functionalized via ATRP. Polymer (Guildf) 55 (20), 5146–5159.

Marla, V.T., Shambaugh, R.L., Papavassiliou, D.V., 2007. Use of an infrared camera for accurate determination of the temperature of polymer filaments. Ind. Eng. Chem. Res. 46 (1), 336–344.

Matthews, F.L., Rawlings, R.D., 1999. Composite Materials: Engineering and Science. CRC press.

Newkirk, J.R., C.M. Degen, and A. Romkes, Characterization of thermoplastic matrix composite joints for the development of a computational framework, in Mechanics of Composite and Multi-functional Materials, *Volume* 6. 2018, Springer. p. 11–19.

Rana, S. and R. Fangueiro, Advanced Composite Materials for Aerospace Engineering: Processing, Properties and Applications. 2016: Woodhead Publishing.

Red, C., 2014. Thermoplastics in aerospace composites outlook. Compos. World 1, 2014–2023.

Tutunjian, S., et al., 2018. Increasing the joint strength of ultrasonic spot welded fiber reinforced laminates by an innovative process control method. In: Proceedings of the 18th European Conference on Composite Materials, Athens, Greece.

Tutunjian, S., et al., 2020a. A numerical analysis of an energy directing method through friction heating during the ultrasonic welding of thermoplastic composites. J. Thermoplast. Compos. Mater. 33 (11), 1569–1587.

Tutunjian, S., et al., 2020b. A numerical analysis of the temporal and spatial temperature development during the ultrasonic spot welding of fibre-reinforced thermoplastics. J. Manuf. Mater. Process. 4 (2), 30.

Villegas, I.F., Bersee, H.E., 2010. Ultrasonic welding of advanced thermoplastic composites: an investigation on energy-directing surfaces. Adv. Polym. Tech. 29 (2), 112–121.

Villegas, I.F., Rans, C., 2021. The dangers of single-lap shear testing in understanding polymer composite welded joints. Philos. Trans. R. Soc. A 379 (2203), 20200296.

Yang, Y., et al., 2012. Recycling of composite materials. Chem. Eng. Process.: Process Intensif. 51, 53–68.

Yousefpour, A., Hojjati, M., Immarigeon, J.-.P., 2004. Fusion bonding/welding of thermoplastic composites. J. Thermoplast. Compos. Mater. 17 (4), 303–341.

Zhang, Z., et al., 2010. Study on heating process of ultrasonic welding for thermoplastics. J. Thermoplast. Compos. Mater. 23 (5), 647–664.

Zhao, Y., Zhang, Y., Lai, X., 2018. Analysis of fracture modes of resistance spot welded hot-stamped boron steel. Metals (Basel) 8 (10), 764.